Journal of Power Sources 261 (2014) 311–316

Contents lists available at ScienceDirect

Journal of Power Sources

journal homepage: www.elsevier.com/locate/jpowsour

Freestanding MnO_2@carbon papers air electrodes for rechargeable Li-O_2 batteries

Leilei Zhang [a,b], Feifei Zhang [a,b], Gang Huang [a,b], Jianwei Wang [a,b], Xinchuan Du [a,b], Yuling Qin [a,b], Limin Wang [a,c,*]

[a] State Key Laboratory of Rare Earth Resource Utilization, Changchun Institute of Applied Chemistry, Chinese Academy of Sciences, 5625 Renmin Street, Changchun 130022, China
[b] University of Chinese Academy of Sciences, Beijing 100049, China
[c] Changzhou Institute of Energy Storage Materials and Devices, Changzhou 213000, China

HIGHLIGHTS

- Freestanding, porous MnO_2@carbon paper (CP) electrodes were prepared.
- We examined electrochemical properties of MnO_2@CP electrode for Li–O_2 batteries.
- MnO_2@CP electrodes improved the reversibility and cycling stability.
- Unique cathode structure contributed the improvement of cell performance.

GRAPHICAL ABSTRACT

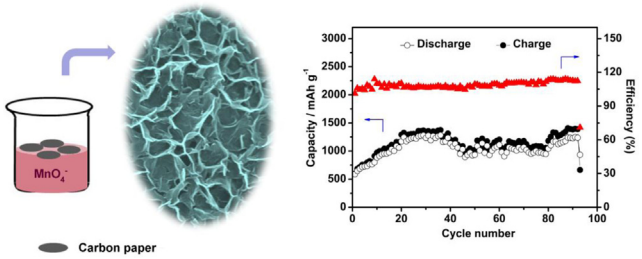

ARTICLE INFO

Article history:
Received 2 December 2013
Received in revised form
12 February 2014
Accepted 20 March 2014
Available online 27 March 2014

Keywords:
Freestanding electrode
MnO_2 nanosheets
Li–O_2 battery
In situ synthesis

ABSTRACT

We have designed the air electrode for rechargeable Li–O_2 batteries by adapting conventional current collectors-carbon papers (CPs), as freestanding substrates. The MnO_2@CP electrodes are prepared by simply floating CPs on $KMnO_4$ solution at room temperature. CPs act as the reducing agents as well as the freestanding substrates. Birnessite-type MnO_2 nanosheets are observed to in situ grow vertically from the surface of CPs, thus building 3D porous architecture. The nanosheets are uniformly distributed and interconnected each other, which contributes to an improved electrical connection among the MnO_2 catalyst and CPs. The cycling tests using the electrode as the cathode in rechargeable Li–O_2 batteries exhibit high reversibility and superior cycling stability, over 90 cycles with a capacity of more than 1000 mA h (g MnO_2)$^{-1}$ and a high coulombic efficiency of around 100% in the voltage rang of 2.2–4.4 V.

1. Introduction

Li–O_2 batteries have attracted extensive attention due to their substantially higher energy density (3505 Wh kg^{-1} based on $2Li + O_2 \rightarrow Li_2O_2$) than conventional lithium-ion batteries [1,2]. However, it is still a great challenge for Li–O_2 batteries to be considered for applications because of their some key problems, including poor cycling stability, low round-trip efficiency, and low rate capacity.

Recent studies have mostly focused on two issues to solve the above problems. The first important measure is to identify a stable electrolyte. Conventional carbonate-based electrolytes are found to decompose easily and generate Li_2CO_3 greatly during cycles [3–5]. Ether-based electrolytes are relatively stable, but are also reported to

* Corresponding author. State Key Laboratory of Rare Earth Resource Utilization, Changchun Institute of Applied Chemistry, Chinese Academy of Sciences, 5625 Renmin Street, Changchun 130022, China. Tel.: +86 431 85262447; fax: +86 431 85262836.
E-mail address: lmwang@ciac.ac.cn (L. Wang).

http://dx.doi.org/10.1016/j.jpowsour.2014.03.094
0378-7753/

decompose upon cycling [6,7]. In addition, some new electrolytes, such as dimethylformamide [8], dimethylacetamide [9], and dimethyl sulfoxide [10] still need further research. The other measurement is to enhance the reaction kinetics by synthesizing a catalyst for oxygen reduction/evolution reaction (ORR/OER) or designing a porous air electrode. The terribly sluggish discharge/charge kinetics not only increases the overpotential, but also causes the pitiful rechargability and low rate capacity. Moreover, the discharge products are insoluble, which will continuously accumulate on the pores of an air electrode, clogging the electrode, thus leading to low capacity. So far, various materials, such as metal oxides, metal nitrides, noble metal, pyrochlore have been reported as catalysts to improve the ORR/OER kinetics [11–16]. However, most of them need to be dispersed on carbon supports with polymeric binders by the mechanical mixing method, subsequently pasted on a porous current collector and formed an air electrode. This conventional fabrication can hardly ensure a uniform dispersion of the catalysts and could cause the electrons disconnecting partly, together with unnecessary side-reactions. To avoid this drawback, freestanding-type cathodes, where additional carbon and binders are no longer necessary, have been introduced and reported to improve the rate capability and cycling stability, including Co_3O_4, graphene oxide, carbon nanotubes, carbon fibers, gold electrode, etc. [17–25].

Manganese oxides (MnO_x) are catalysts commonly used in the cathodes of Li–O_2 batteries. However, the freestanding cathodes of Li–O_2 batteries with MnO_x have rarely been reported. Herein, we propose a simple strategy to grow porous MnO_2 nanosheets on carbon papers (CPs) to prepare freestanding MnO_2@CP electrodes via a facile and cost-effective in situ redox process at room temperature, according to a well-known reaction of $4MnO_4^- + 3C + H_2O \rightarrow 4MnO_2 + CO_3^{2-} + 2HCO_3^-$. The fabrication scheme is displayed in Fig. 1. Floating CPs on $KMnO_4$ solution, the side of CPs facing the $KMnO_4$ solution will be coated by MnO_2, while the other side facing air will still keep the original structure. In this study, CPs act as reducing agents as well as current collectors. Therefore, the fabrication scheme not only favors the efficiency of catalysts, but also guarantees the electrical conductivity of CPs as current collectors. Furthermore, there are other attractive benefits for Li–O_2 batteries as follows: i) free binders increase the electrical conduction and decrease side-reactions induced by binders (such as PVDF) [26]; ii) MnO_2 is obtained by in situ reaction with CPs, thereby ensuring good enough contact and reducing the contact resistance between them; iii) the MnO_2@CP will inherit the porous morphology of CPs to guarantee the flow of O_2. Based on the above features, the MnO_2@CP shows unique performance.

2. Experimental

2.1. Preparation of MnO_2@CP

All the chemical reagents were analytical grade and used without further purification. The MnO_2@CP electrodes were prepared by floating the CPs on $KMnO_4$ solution at room temperature. In a typical procedure, the CPs (Dong Li 060) were firstly cut into small disks with a diameter of 12 mm. Then, the disks were treated in the mixture of concentrated sulfuric acid and concentrated nitric acid (V:V = 3:1) at 70 °C for 3 h. After washing with water and drying, four disks were floating on 20 mL $KMnO_4$ solution (10 mg $KMnO_4$) in a 100-mL beaker for 24 h. The amount of MnO_2 was about 1 mg, which was calculated by dissolving the MnO_2 in 3 M HCl.

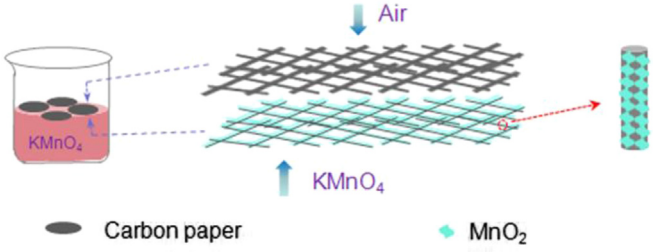

Fig. 1. Fabrication scheme of the MnO_2@CP electrode.

2.2. Characterization of the electrodes

X-ray diffraction (XRD) patterns were collected using Bruker D8 Focus Powder X-ray diffractometer with a Cu Kα X-ray radiation (40 kV, 40 mA). Scanning electrode microscopy (SEM) images were recorded on a Hitachi S-4800 field emission scanning electron microscopy. X-ray photoelectron spectroscopy (XPS) spectra were acquired using an Escalab X-ray photoelectron spectrometer with a monochromatic Al Kα X-ray radiation. Raman spectra were collected with a micro-Raman spectrometer (Renishaw) with a laser of 532 nm wavelength.

2.3. Electrochemical measurements

Electrochemical characterizations of Li–O_2 cells were carried out using 2025-type coin cells composed of a lithium metal anode (Φ13.6 × 0.5 mm), a glass fiber separator impregnated with 0.07 mL electrolyte composed of 1 M lithium trifluoromethane sulfonate ($LiCF_3SO_3$) in tetraethylene glycol dimethyl ether (TEGDME), and a synthesized MnO_2@CP cathode. The cells were sealed except holes of the cathode shell exposed to 1 atm O_2 environment. The galvanostatic discharge-charge tests were conducted with a LAND CT2001A multi-channel battery testing system with the voltage window of 2.2–4.4 V.

Mixed MnO_2 cathodes were prepared by the conventional process, brushing the mixture of 80 wt.% commercial MnO_2 powders and 20 wt.% Li-Nafion binders on CPs. The processes of assembling and testing the Li–O_2 cells were the same as that of MnO_2@CP.

2.4. Characterization of discharge/charge products

The cells after cycles were disassembled in the argon-filled glove box. MnO_2@CP cathodes were ringed three times with dimethoxyethane (DME), dried under vacuum, and then introduced into the SEM, XRD and Fourier transform infrared spectroscopy (FTIR, BRUKER Vertex 70 spectrometer).

3. Results and discussion

CPs, owning porous skeleton and stability, are popular current collectors for Li–O_2 batteries. The porous and interconnected morphology of CPs with a smooth surface is shown in Fig. 2a and b. From the inset optical images, we can see that the color of the CPs changed from gray to dark black after reacting with $KMnO_4$, suggesting the successful reaction. SEM images of the MnO_2@CP shown in Fig. 2c and d demonstrates that the porous nanosheets homogenously cover the exposed surface of CPs and the smooth surface is changed to 3D network, while the porous and interconnected skeletons of CPs are preserved as the origin, which are consistent with the surmise in introduction. From a higher magnification SEM image shown in Fig. 2f, we can clearly see the growth of the nanosheets. The nanosheets vertically grow at the exposed surfaces of the CPs, disperse uniformly, interconnected, and form an inseparable unity with the CPs.

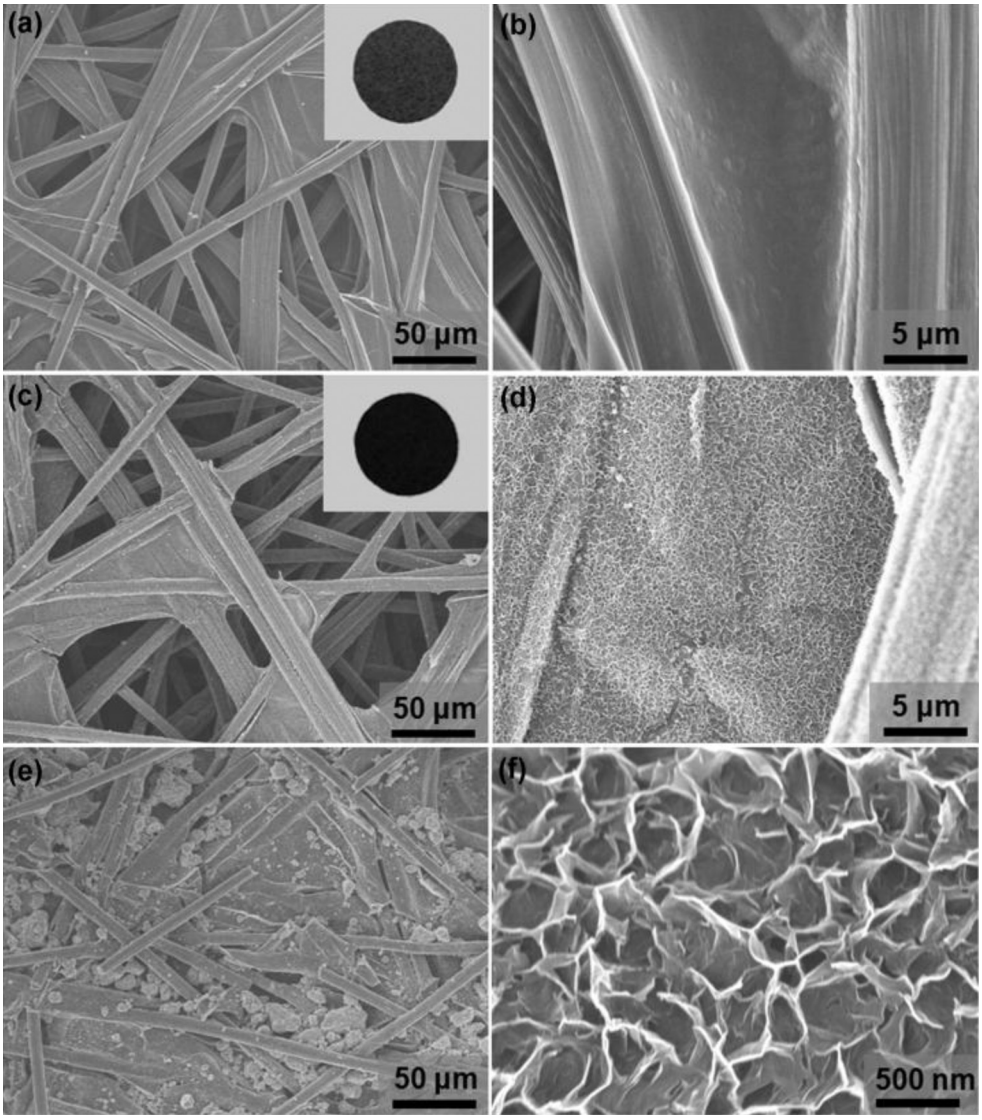

Fig. 2. (a, b) SEM images of the pristine CP (inset a: optical image). (c, d) SEM images of the synthesized MnO_2@CP (inset c: optical image). (e) SEM image of the mixed MnO_2 electrode. (f) High magnification SEM image of the MnO_2@CP.

Fig. 2e shows the SEM image of the mixed MnO_2 cathode. Like other conventional Li–O_2 cathodes, MnO_2 powders stacked randomly on the surface of the CPs, or accumulated in the void of carbon fibers. The porosity of the CPs was obviously destroyed.

The crystallographic structure of the synthesized MnO_2@CP was investigated by XRD and Raman measurements. Fig. 3a shows the XRD patterns of the CP and the MnO_2@CP. Aside from the peaks of the CP, a broad peak at 2θ around 12° is observed. The peak may be indexed to the birnessite-type MnO_2 (JCPDS No. 80-1098) [27,28]. Although the XRD results can demonstrate the formation of MnO_2, the peak is too weak to explain the crystallographic structure clearly. For this reason, Raman was conducted and the results are shown in Fig. 3b, which further confirm the synthesis of MnO_2. The spectra around 500 cm^{-1}, 575 cm^{-1} and 640 cm^{-1} are in good agreement with the birnessite-type MnO_2 [28–30]. In addition, the birnessite-type MnO_2 has the crystallographic habit to develop sheet morphology [31], which accords with the SEM images.

XPS measurements were carried out to confirm the chemical state of the MnO_2 and the data are shown in Fig. 4. The binding energy peaks of Mn $2p_{3/2}$ and Mn $2p_{1/2}$ are located at 642.3 eV and 654.1 eV, respectively, with a spin energy separation of 11.8 eV. A separate energy of 4.8 eV for Mn 3s suggests that the oxidation state of the Mn is around 4.0. A peak of O 1s spectra at 530 eV corresponds to the oxide lattice ion (Mn–O–Mn), whereas the peak at 532 eV is related to Mn–O–H bond. The XPS data are coincident with previously reported values about MnO_2 [32,33].

The synthesized MnO_2@CP was used as a cathode for the Li–O_2 cell directly. 1 M $LiCF_3SO_3$ in TEGDME was chosen as the electrolyte since it is comparatively stable [6,15,25,26,34,35]. Fig. 5a shows the 80 cycles discharge/charge curves in the voltage rang of 2.2–4.4 V at the current density of 0.1 mA cm^{-2}. The specific capacity is normalized with the mass of MnO_2. The discharge potential plateau is kept around 2.68 V, while the charge potential plateau is kept around 4.15 V. Besides, the electrochemical profiles do not change significantly over cycles. These clearly indicate that the cell can be reversibly discharged/charged and the MnO_2@CP has a good cycle performance. Fig. 5b shows the cycling stability and coulombic efficiency of the cell with the MnO_2@CP. The discharge capacity increases gradually from 500 to 1000 mAh g^{-1} on the first 20 cycles, which may due to the activation, and then sustains at above 1000 mAh g^{-1} on the subsequent cycles. Meanwhile, the corresponding coulombic efficiency is always around 100%. It should be

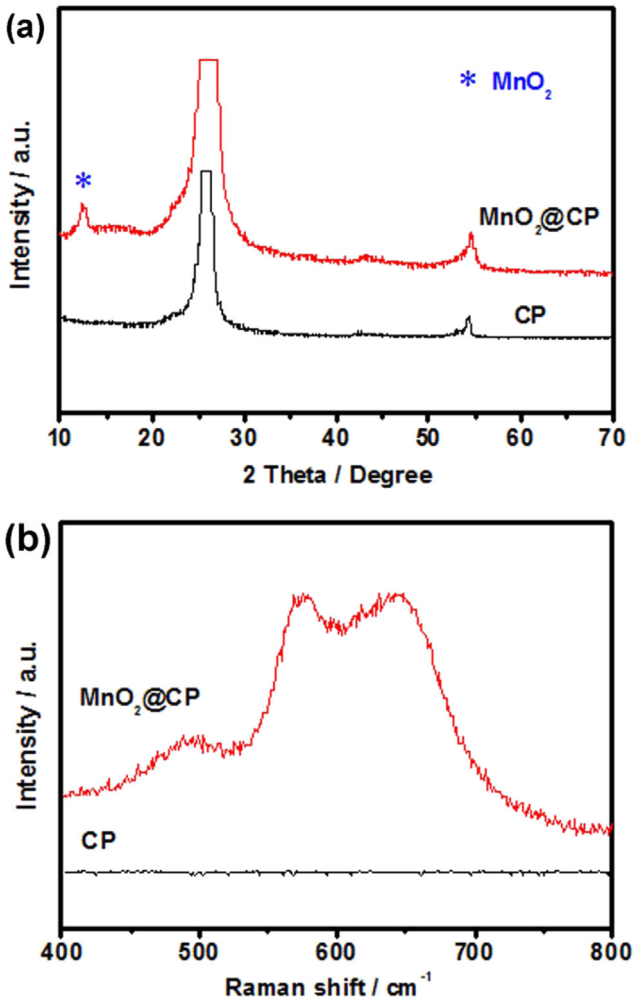

Fig. 3. XRD patterns (a) and Raman spectra (b) of the MnO_2@CP.

noted that most of the results reported so far concerning good cycle performance of Li–O_2 cells are tested with a limited capacity or high discharge voltage to avoid deep discharge. Once with a deep or full discharge, the charge capacity will dramatically decrease and the cycle will be hard to continue. In this work, we discharged the cell to a low voltage of 2.2 V and did not limit the capacity. Therefore, the cycling performance of the MnO_2@CP is unique and excellent because of its long cycle time accompanied with high coulombic efficiency under deep discharge. Moreover, except 70 mAh g^{-1} from the Li intercalation (the figure is not display), the capacity is due to the reaction of lithium and oxygen, and the

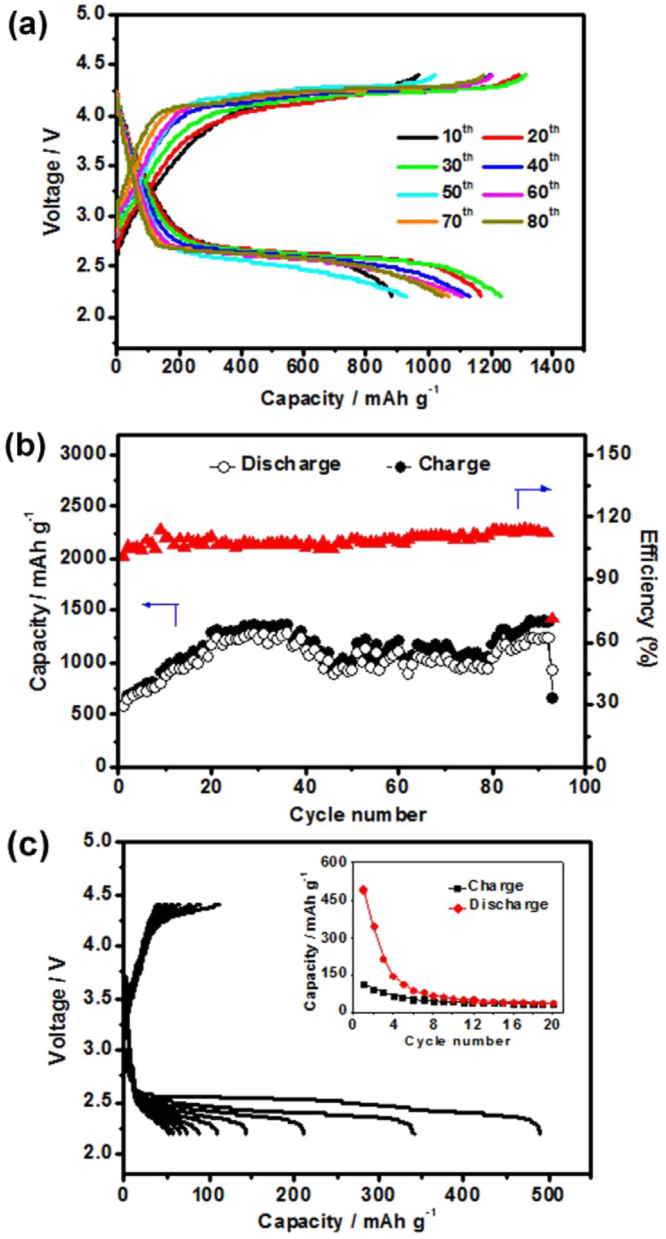

Fig. 5. Discharge/charge profiles (a) and cycle performance (b) of Li–O_2 cells with the MnO_2@CP cathode at a current density of 0.1 mA cm^{-2}. (c) Discharge/charge profiles of the cell with mixed MnO_2 cathode (inset: capacity *vs.* cycle number graph).

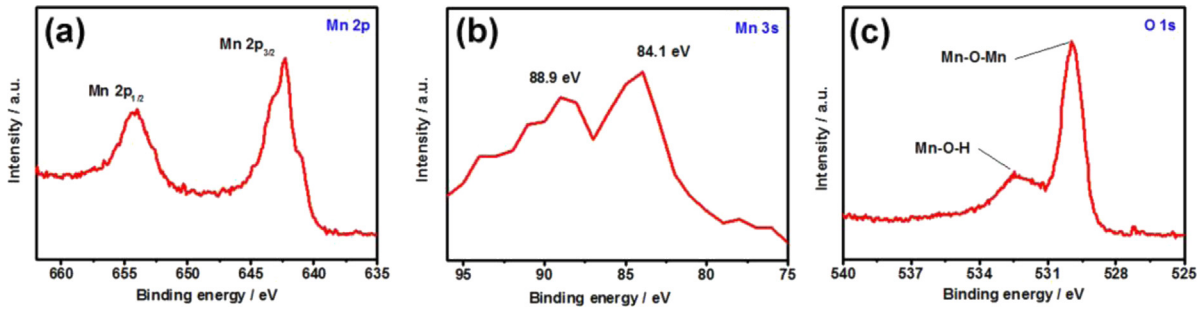

Fig. 4. XPS results of the MnO_2@CP: (a) Mn 2p spectrum; (b) Mn 3s spectrum; (c) O 1s spectrum.

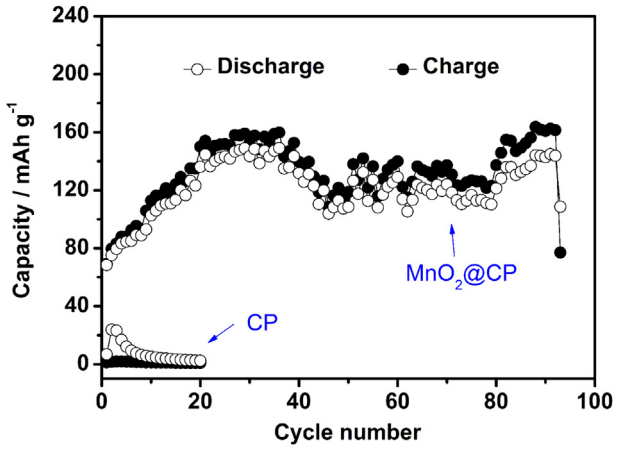

Fig. 6. Discharge/charge profiles of Li–O_2 cells with the MnO_2@CP cathode and pure CP electrode without MnO_2, based on the total electrode mass. The current density is 0.1 mA cm^{-2}.

discharge capacity value of the cells is competitive in non-carbon Li–O_2 batteries. For comparison, we fabricated mixed MnO_2 cathodes by the conventional process. As shown in Fig. 5c, the mixed MnO_2 cathodes delivers a comparable first discharge capacity of 500 mAh g^{-1}. However, the charge capacity is pitiful and the following discharge capacity decays fast. The specific capacity normalized with the total mass of the MnO_2@CP electrode (MnO_2 + CP) is shown in Fig. 6. Compared with that of the pure CP without MnO_2, the MnO_2@CP improves the specific capacity and cycle stability greatly.

Fig. 7 shows the Li–O_2 performance of the MnO_2@CP at a much higher current density of 0.3 mA cm^{-2}. The cell can cycle 100 times with a relatively stable capacity of 600 mAh g^{-1} and keep around 100% coulombic efficiency, showing the outstanding cycling stability and good rate capability.

The SEM image of the discharged MnO_2@CP electrode is shown in Fig. 8a, which demonstrates that the discharge products deposit on the surface of MnO_2 nanosheets. They form a homogenous film coating the MnO_2 catalysts without any accumulation or clogging. The discharge product morphology illustrates a high uniform dispersion of the products which is explained in our previous report [36]. Besides, from the SEM image of the charged MnO_2@CP electrode shown in Fig. 8b, we can see that the film disappears thoroughly and the nanosheets recover the smooth surface, indicating the high reversibility of the electrodes.

XRD patterns (Fig. 9a) show that LiOH is formed after discharge, which can reversibly decompose during charge. Meanwhile, FTIR spectra, shown in Fig. 9b, demonstrate that Li_2O_2, Li_2CO_3 are formed alongside of LiOH, and they are all removed during the following charge process. Based on former reports about the formation of LiOH in Li–O_2 battery [23,26,37], we speculate two reasons for why there is a significant quantity of LiOH in our study. The first one is the –OH group on the surface of the MnO_2@CP (Fig. 4c). The other one may be because of the catalytic effect of MnO_2 nanosheets, which result in some discharge product particles growing too small to be characterized. As to the dependence of the electrolyte, it

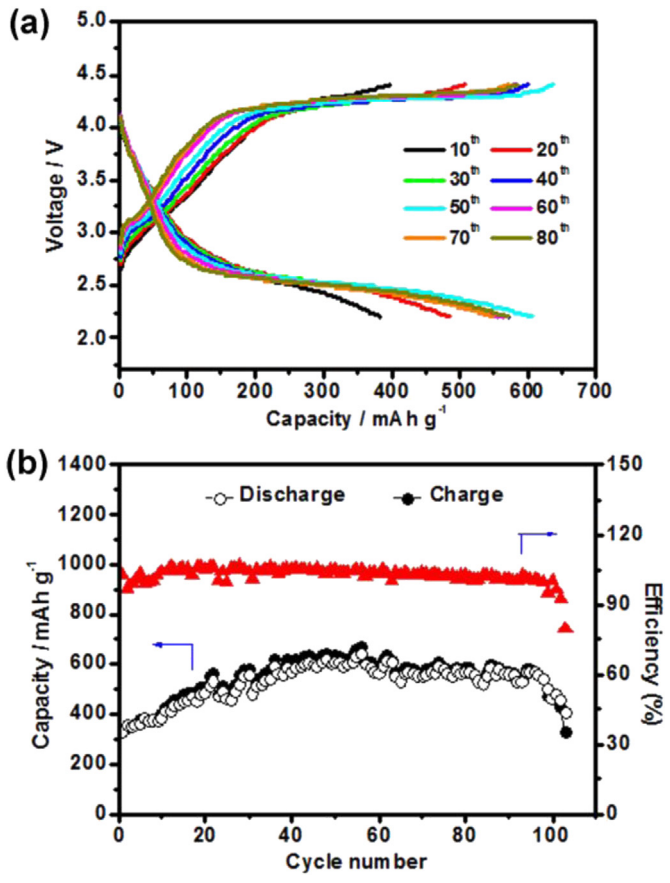

Fig. 7. Discharge/charge profiles (a) and cycle performance (b) of Li–O_2 cells with the MnO_2@CP cathode at a current density of 0.3 mA cm^{-2}.

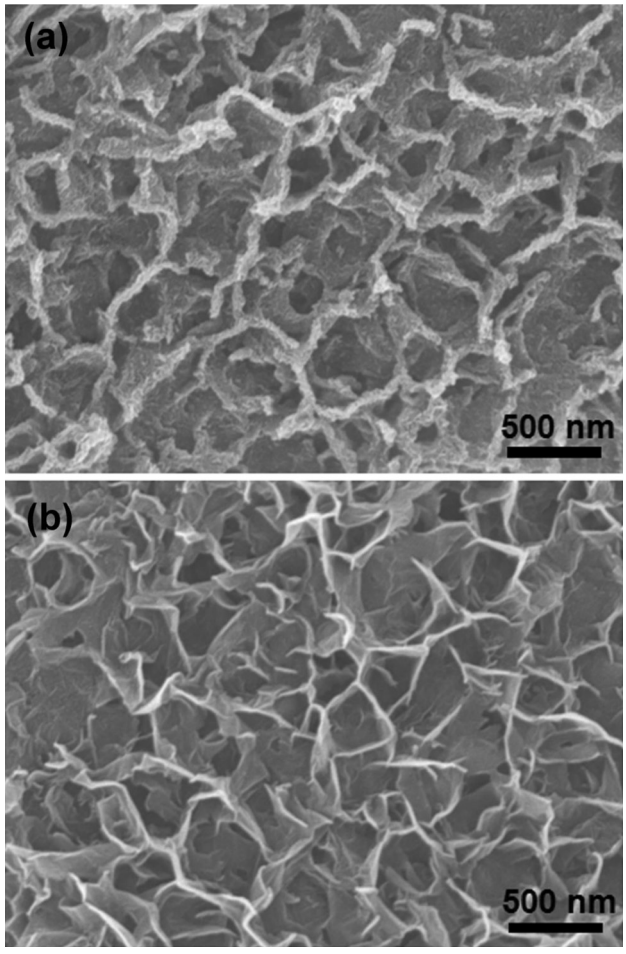

Fig. 8. SEM images of the MnO_2@CP cathodes after first discharge (a) and charge (b).

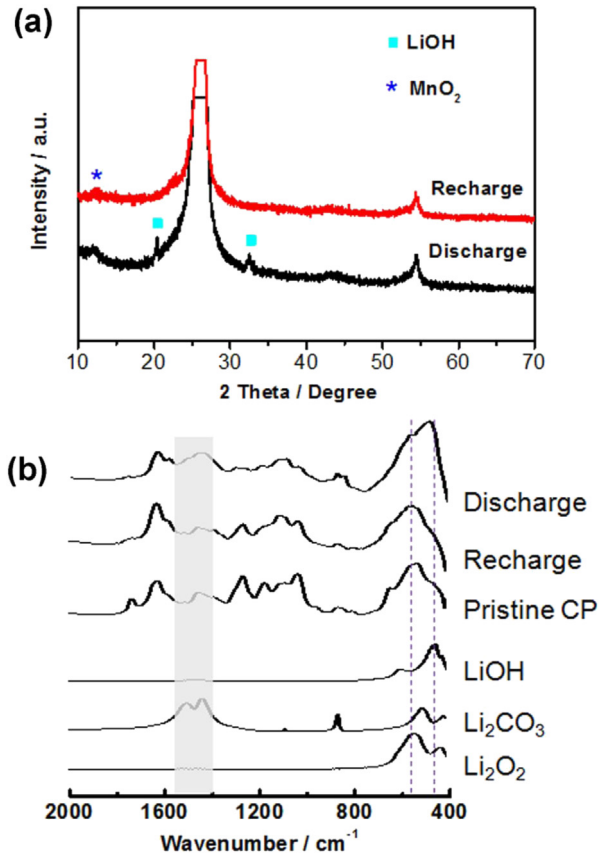

Fig. 9. XRD patterns (a) and FTIR spectra (b) of the MnO_2@CP cathodes after discharge and charge.

deserves further study. Nevertheless, the MnO_2@CP cathodes improve the reversibility of Li—O_2 cells.

The super reversibility and cycling stability of the MnO_2@CP are not only attributed to the three features mentioned in the introduction, but also due to the 3D porous structure of MnO_2 nanosheets [17,18,38]. Firstly, the vertically grown MnO_2 nanosheets can expose their catalytic sites maximally and promote a uniform dispersion of the discharge products. Secondly, the porous framework ensures the flow of gases, allowing the oxygen to get in touch with the catalysts adequately. Thirdly, the interconnected MnO_2 network could guide the electrolyte to wet the catalyst successively, prompting lithium ions to access the inner space of MnO_2 catalysts. Therefore, because of the close contact between the reactants and catalysts, the ORR/OER kinetics is improved, resulting to high reversibility even at deep discharge. Furthermore, the porous structure provides enough space for products deposition, prevents them accumulation, and ultimately increases the discharge capacity.

4. Conclusions

In summary, we have designed a freestanding MnO_2@CP air electrode with 3D porous catalytic network structures as the cathode for Li—O_2 batteries. The synthesis of the MnO_2@CP realizes the in situ growth of catalysts on current collectors by using the current collectors as reducing agents, increasing the contact strength. The Li—O_2 cells with the MnO_2@CP cathodes can be reversibly discharged/charged and have an excellent cycling stability under low discharge voltage. The discharge products homogenously deposit on the surface of MnO_2 nanosheets forming a uniform film. The superior enhancement can be ascribed to the unique porous structure of MnO_2 nanosheets and the intrinsic contact between them and CPs. Further work is needed to understand the electrochemical process in cycles in Li—O_2 batteries.

Acknowledgments

This work is financially supported by the National Natural Science Foundation of China (Grant No. 21101147 and 21203176), and the Foundation for Innovative Research Groups of the National Natural Science Foundation of China (Grant No. 20921002).

References

[1] K.M. Abraham, Z. Jiang, J. Electrochem. Soc. 143 (1996) 1.
[2] P.G. Bruce, S.A. Freunberger, L.J. Hardwick, J.M. Tarascon, Nat. Mater. 11 (2012) 19.
[3] S.A. Freunberger, Y. Chen, Z. Peng, J.M. Griffin, L.J. Hardwick, F. Barde, P. Novak, P.G. Bruce, J. Am. Chem. Soc. 133 (2011) 8040.
[4] B. McCloskey, D. Bethune, R. Shelby, G. Girishkumar, A. Luntz, J. Phys. Chem. Lett. 2 (2011) 1161.
[5] W. Xu, K. Xu, V.V. Viswanathan, S.A. Towne, J.S. Hardy, J. Xiao, Z. Nie, D. Hu, D. Wang, J.G. Zhang, J. Power Sources 196 (2011) 9631.
[6] S.A. Freunberger, Y. Chen, N.E. Drewett, L.J. Hardwick, F. Bardé, P.G. Bruce, Angew. Chem. Int. Ed. 50 (2011) 8609.
[7] C. Laoire, S. Mukerjee, E.J. Plichta, M.A. Hendrickson, K. Abraham, J. Electrochem. Soc. 158 (2011) A302.
[8] Y. Chen, S.A. Freunberger, Z. Peng, F. Bardé, P.G. Bruce, J. Am. Chem. Soc. 134 (2012) 7952.
[9] W. Walker, V. Giordani, J. Uddin, V.S. Bryantsev, G.V. Chase, D. Addison, J. Am. Chem. Soc. 135 (2013) 2076.
[10] D. Xu, Z. Wang, J. Xu, L. Zhang, L. Wang, X. Zhang, Chem. Commun. 48 (2012) 11674.
[11] S. Ida, A.K. Thapa, Y. Hidaka, Y. Okamoto, M. Matsuka, H. Hagiwara, T. Ishihara, J. Power Sources 203 (2012) 159.
[12] W. Yang, J. Salim, C. Ma, Z. Ma, C. Sun, J. Li, L. Chen, Y. Kim, Electrochem. Commun. 28 (2013) 13.
[13] F. Li, Y. Yamada, J. Kubota, K. Domen, A. Yamada, H. Zhou, Chem. Commun. 49 (2013) 1175.
[14] Y.-C. Lu, Z. Xu, H.A. Gasteiger, S. Chen, K. Hamad-Schifferli, Y. Shao-Horn, J. Am. Chem. Soc. 132 (2010) 12170.
[15] S.H. Oh, R. Black, E. Pomerantseva, J.H. Lee, L.F. Nazar, Nat. Chem. 4 (2012) 1004.
[16] J. Xu, D. Xu, Z. Wang, H. Wang, L. Zhang, X. Zhang, Angew. Chem. Int. Ed. 52 (2013) 3887.
[17] Y. Cui, Z. Wen, Y. Liu, Energy Environ. Sci. 4 (2011) 4727.
[18] Z.L. Wang, D. Xu, J.J. Xu, L.L. Zhang, X.B. Zhang, Adv. Funct. Mater. 22 (2012) 3699.
[19] H. Wang, K. Xie, L. Wang, Y. Han, RSC Adv. 3 (2013) 8236.
[20] H.D. Lim, K.Y. Park, H. Song, E.Y. Jang, H. Gwon, J. Kim, Y.H. Kim, M.D. Lima, R.O. Robles, X. Lepró, Adv. Mater. 25 (2013) 1348.
[21] Y. Chen, F. Li, D.-M. Tang, Z. Jian, C. Liu, D. Golberg, A. Yamada, H. Zhou, J. Mater. Chem. A 1 (2013) 13076.
[22] R.R. Mitchell, B.M. Gallant, C.V. Thompson, Y. Shao-Horn, Energy Environ. Sci. 4 (2011) 2952.
[23] Z. Peng, S.A. Freunberger, Y. Chen, P.G. Bruce, Science 337 (2012) 563.
[24] A. Riaz, K.-N. Jung, W. Chang, S.-B. Lee, T.-H. Lim, S.-J. Park, R.-H. Song, S. Yoon, K.-H. Shin, J.-W. Lee, Chem. Commun. 49 (2013) 5984.
[25] H.-G. Jung, J. Hassoun, J.-B. Park, Y.-K. Sun, B. Scrosati, Nat. Chem. 4 (2012) 579.
[26] R. Black, S.H. Oh, J.-H. Lee, T. Yim, B. Adams, L.F. Nazar, J. Am. Chem. Soc. 134 (2012) 2902.
[27] J. Liu, J. Jiang, C. Cheng, H. Li, J. Zhang, H. Gong, H.J. Fan, Adv. Mater. 23 (2011) 2076.
[28] C. Julien, M. Massot, R. Baddour-Hadjean, S. Franger, S. Bach, J.P. Pereira-Ramos, Solid State Ionics 159 (2003) 345.
[29] K.-W. Nam, K.-B. Kim, J. Electrochem. Soc. 153 (2006) A81.
[30] J. Wang, Y. Yang, Z. Huang, F. Kang, J. Power Sources 224 (2013) 86.
[31] W. Xiao, D. Wang, X.W. Lou, J. Phys. Chem. C 114 (2009) 1694.
[32] J. Gomez, E.E. Kalu, R. Nelson, M.H. Weatherspoon, J.P. Zheng, J. Mater. Chem. A 1 (2013) 3287.
[33] L. Bao, J. Zang, X. Li, Nano Lett. 11 (2011) 1215.
[34] V.S. Bryantsev, V. Giordani, W. Walker, M. Blanco, S. Zecevic, K. Sasaki, J. Uddin, D. Addison, G.V. Chase, J. Phys. Chem. A 115 (2011) 12399.
[35] Z. Zhang, J. Lu, R.S. Assary, P. Du, H.H. Wang, Y.K. Sun, Y. Qin, K.C. Lau, J.P. Greeley, P.C. Redfern, J. Phys. Chem. C 115 (2011) 25535.
[36] J.J. Xu, Z.L. Wang, D. Xu, L.L. Zhang, X.B. Zhang, Nat. Commun. 4 (2013) 2438.
[37] M.M. Ottakam Thotiyl, S.A. Freunberger, Z. Peng, P.G. Bruce, J. Am. Chem. Soc. 135 (2013) 494.
[38] L. Zhang, X. Zhang, Z. Wang, J. Xu, D. Xu, L. Wang, Chem. Commun. 48 (2012) 7598.